

# FFDNet: Toward a Fast and Flexible Solution for CNN based Image Denoising

Kai Zhang, Wangmeng Zuo, *Senior Member, IEEE*, and Lei Zhang *Senior Member, IEEE*

**Abstract**—Due to the fast inference and good performance, discriminative learning methods have been widely studied in image denoising. However, these methods mostly learn a specific model for each noise level, and require multiple models for denoising images with different noise levels. They also lack flexibility to deal with spatially variant noise, limiting their applications in practical denoising. To address these issues, we present a fast and flexible denoising convolutional neural network, namely FFDNet, with a tunable noise level map as the input. The proposed FFDNet works on downsampled sub-images to speed up the inference, and adopts orthogonal regularization to enhance the generalization ability. In contrast to the existing discriminative denoisers, FFDNet enjoys several desirable properties, including (i) the ability to handle a wide range of noise levels (i.e., [0, 75]) effectively with a single network, (ii) the ability to remove spatially variant noise by specifying a non-uniform noise level map, and (iii) faster speed than benchmark BM3D even on CPU without sacrificing denoising performance. Extensive experiments on synthetic and real noisy images are conducted to evaluate FFDNet in comparison with state-of-the-art denoisers. The results show that FFDNet is effective and efficient, making it highly attractive for practical denoising applications.

**Index Terms**—Image denoising, convolutional neural networks, residual learning, spatially variant noise

## I. INTRODUCTION

IMAGE denoising is a typical inverse problem in low level vision. Noise corruption is inevitable during the image sensing process and it may heavily degrade the quality of acquired image. Removing noise from the observed image is an essential step in various image processing and computer vision tasks [1], [2]. On the other hand, from the Bayesian perspective, image denoising is an ideal test bed for evaluating image prior models and optimization methods [3], [4], [5]. Moreover, in the unrolled inference via variable splitting techniques, many image restoration problems can be addressed by sequentially solving a series of denoising subproblems, which further broadens the application fields of image denoising [6], [7], [8], [9].

As in many previous literature of image denoising [10], [11], [12], [13], in this paper we assume that the noise is

additive white Gaussian noise (AWGN) and the noise level is given. In order to handle practical image denoising problems, a flexible image denoiser is expected to have the following desirable properties: (i) it is able to perform denoising using a single model; (ii) it is efficient, effective and user-friendly; and (iii) it can handle spatially variant noise. Such a denoiser can be directly deployed to recover the clean image when the noise level is known or can be well estimated. When the noise level is unknown or is difficult to estimate, the denoiser should allow the user to adaptively control the tradeoff between noise reduction and details preservation. Furthermore, the noise can be spatially variant and the denoiser should be flexible enough to handle spatially variant noise.

However, state-of-the-art image denoising methods are still limited in flexibility or efficiency. In general, image denoising methods can be grouped into two major categories, model-based methods and discriminative learning based ones. Model-based methods such as BM3D [11] and WNNM [5] are flexible in handling denoising problems with various noise levels, but they suffer from several drawbacks. For example, their optimization algorithms are generally time-consuming, and cannot be directly used to remove spatially variant noise. Moreover, model-based methods usually employ hand-crafted image priors (e.g., sparsity [14], [15] and nonlocal self-similarity [12], [13], [16]), which may not be strong enough to characterize complex image structures.

As an alternative, discriminative denoising methods aim to learn the underlying image prior and fast inference from a training set of degraded and ground-truth image pairs. One approach is to learn stage-wise image priors in the context of truncated inference procedure [17]. Another more popular approach is plain discriminative learning, such as the MLP [18] and convolutional neural network (CNN) based methods [19], [20], among which the DnCNN [20] method has achieved very competitive denoising performance. The success of CNN for image denoising is attributed to its large modeling capacity and tremendous advances in network training and designing. However, existing discriminative denoising methods are limited in flexibility, and the learned model is usually tailored to a specific noise level. From the perspective of regression, they aim to learn a mapping function  $\mathbf{x} = f(\mathbf{y}; \Theta_\sigma)$  between the input noisy observation  $\mathbf{y}$  and the desired output  $\mathbf{x}$ . The model parameters  $\Theta_\sigma$  are trained for noisy images corrupted by AWGN with a fixed noise level  $\sigma$ , while the trained model with  $\Theta_\sigma$  is hard to be directly deployed to images with other noise levels. Though a single CNN model (i.e., DnCNN-B) is trained in [20] for Gaussian denoising, it does not generalize well to real noisy images and works only if the noise level

This project is partially supported by the National Natural Scientific Foundation of China (NSFC) under Grant No. 61671182 and 61471146, and the HK RGC GRF grant (under no. PolyU 5313/13E).

K. Zhang is with the School of Computer Science and Technology, Harbin Institute of Technology, Harbin 150001, China, and also with the Department of Computing, The Hong Kong Polytechnic University, Hong Kong (e-mail: cskazhang@gmail.com).

W. Zuo is with the School of Computer Science and Technology, Harbin Institute of Technology, Harbin 150001, China (e-mail: cswmzuo@gmail.com).

L. Zhang is with the Department of Computing, The Hong Kong Polytechnic University, Hong Kong (e-mail: cslzhang@comp.polyu.edu.hk).

is in the preset range, e.g., [0, 55]. Besides, all the existing discriminative learning based methods lack flexibility to deal with spatially variant noise.

To overcome the drawbacks of existing CNN based denoising methods, we present a fast and flexible denoising convolutional neural network (FFDNet). Specifically, our FFDNet is formulated as  $\mathbf{x} = f(\mathbf{y}, \mathbf{m}; \Theta)$ , where  $\mathbf{m}$  is a noise level map. In the DnCNN model  $\mathbf{x} = f(\mathbf{y}; \Theta_\sigma)$ , the parameters  $\Theta_\sigma$  vary with the change of noise level  $\sigma$ , while in the FFDNet model, the noise level map is modeled as an input and the model parameters  $\Theta$  are invariant to noise level. FFDNet provides a flexible way to handle various types of noise with a single network.

By introducing a noise level map as input, new network design and training methods are required for an effective and efficient denoising solution. It is found that heavy visual quality degradation may be engendered by the mismatching between the input noise level and the ground truth one. To address this issue, we propose to impose an orthogonal regularization on convolutional filters during network training in addition to adopting batch normalization and residual learning [20]. Meanwhile, the proposed FFDNet works on downsampled sub-images, which largely accelerates the training and testing speed, and enlarges the receptive field as well.

Using images corrupted by AWGN, we quantitatively compare FFDNet with state-of-the-art denoising methods, including model-based methods such as BM3D [11] and WNNM [5] and discriminative learning based methods such as TNRD [17] and DnCNN [20]. The results clearly demonstrate the superiority of FFDNet in terms of both denoising accuracy and computational efficiency. In addition, FFDNet performs favorably on images corrupted by spatially variant AWGN. We further evaluate FFDNet on real-world noisy images, where the noise is often signal-dependent, non-Gaussian and spatially variant. The proposed FFDNet model still achieves perceptually convincing results. Overall, FFDNet enjoys high potentials for practical denoising applications.

The main contribution of our work is summarized as follows:

- A fast and flexible denoising network, namely FFDNet, is proposed for discriminative image denoising. By taking a tunable noise level map as input, a single FFDNet is able to deal with noise on different levels, as well as spatially variant noise.
- An orthogonal regularization method is proposed to improve the robustness of FFDNet to the mismatching between input and ground truth noise levels.
- FFDNet exhibits perceptually appealing results on both synthetic noisy images corrupted by AWGN and real-world noisy images, demonstrating its potentials on practical image denoising.

The remainder of this paper is organized as follows. Sec. II reviews existing discriminative denoising methods. Sec. III presents the proposed image denoising model. Sec. IV reports the experimental results. Sec. V concludes the paper with some discussions on future work.

## II. RELATED WORK

In this section, we briefly review and discuss the two major categories of relevant methods to this work, i.e., maximum a posteriori (MAP) inference guided discriminative learning and plain discriminative learning.

### A. MAP Inference Guided Discriminative Learning

Instead of first learning the prior and then performing the inference, this category of methods aim to learn the prior parameters along with a compact unrolled inference through minimizing a loss function [21]. Following the pioneer work of fields of experts [3], Barbu [21] trained a discriminative Markov random field (MRF) model together with a gradient descent inference for image denoising. Samuel and Tappen [22] independently proposed a compact gradient descent inference learning framework, and discussed the advantages of discriminative learning over model-based optimization method with MRF prior. Sun and Tappen [23] proposed a novel nonlocal range MRF (NLR-MRF) framework, and employed the gradient-based discriminative learning method to train the model. Generally speaking, the methods above only learn the prior parameters in a discriminative manner, while the inference parameters are stage-invariant.

With the aid of unrolled half quadratic splitting (HQS) techniques, Schmidt et al. [24] proposed a cascade of shrinkage fields (CSF) framework to learn stage-wise inference parameters. Chen et al. [17] further proposed a trainable nonlinear reaction diffusion (TNRD) model through discriminative learning of a compact gradient descent inference step. Recently, Lefkimmiatis [25] adopted a proximal gradient-based denoising inference from a variational model to incorporate the nonlocal self-similarity prior.

MAP inference guided discriminative learning usually requires much fewer inference steps, and is very efficient in image denoising. It also has clear interpretability because the discriminative architecture is derived from optimization algorithms such as HQS and gradient descent [17], [21], [22], [23], [24]. However, the learned priors and inference procedure are limited by the form of MAP model, which may be insufficient in modeling complex image priors [20]. The unrolled inference actually can be viewed as a network with stage-wise architecture, which restricts the dataflow in each immediate output layer [9]. In addition, MAP inference guided discriminative learning lacks flexibility in handling spatially variant noise.

### B. Plain Discriminative Learning

Instead of modeling image priors explicitly, the plain discriminative learning methods learn a direct mapping function to model image prior implicitly. The multi-layer perceptron (MLP) and CNNs have been adopted to learn such priors. The use of CNN for image denoising can be traced back to [19], where a five-layers network with sigmoid nonlinearity was proposed. Subsequently, auto-encoder based methods have been suggested for image denoising [26], [27]. However, early MLP and CNN-based methods are limited in denoising

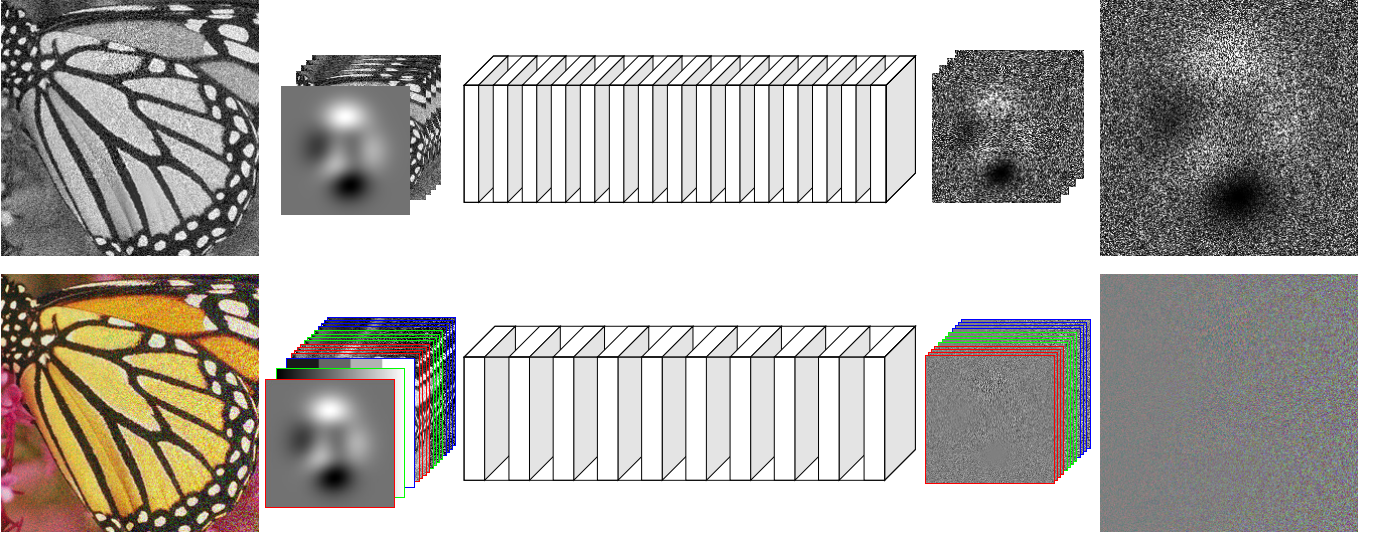


Fig. 1. The architectures of the proposed FFDNet for gray level image denoising (top) and color image denoising (bottom). The input image is reshaped to four sub-images, which are then input to the CNN together with a noise level map. The network output approximates the residual between the input noisy image and the ground-truth clean image.

performance and cannot compete with the benchmark BM3D method [11].

The first discriminative denoising method which achieves comparable performance with BM3D is the plain MLP method proposed by Burger et al. [18]. Benefitted from the advances in deep CNN, Zhang et al. [20] proposed a plain denoising CNN (DnCNN) method which achieves state-of-the-art denoising performance. They showed that residual learning and batch normalization [28] are particularly useful for the success of denoising. For a better tradeoff between accuracy and speed, Zhang et al. [9] introduced a 7-layer denoising network with dilated convolution [29] to expand the receptive field of CNN. Santhanam et al. [30] developed a recursively branched deconvolutional network (RBDN) for image denoising as well as generic image-to-image regression.

Plain discriminative learning has shown better performance than MAP inference guided discriminative learning; however, existing discriminative learning methods have to learn multiple models for handling images with different noise levels, and are incapable to deal with spatially variant noise. To the best of our knowledge, it remains an unaddressed issue to develop a single discriminative denoising model which can handle noise of different levels, even spatially variant noise, in a speed even faster than BM3D.

### III. PROPOSED FAST AND FLEXIBLE DISCRIMINATIVE CNN DENOISER

We present a single discriminative CNN model, namely FFDNet, to achieve the following three objectives:

- **Fast speed:** The denoiser is expected to be highly efficient without sacrificing denoising performance.
- **Flexibility:** The denoiser is able to handle images with different noise levels and even spatially variant noise.
- **Robustness:** The denoiser should be robust to the estimation error of noise levels.

In this work, we take a tunable noise level map  $\mathbf{m}$  as input to make the denoising model flexible to noise levels. To improve the efficiency of the denoiser, a reversible downsampling operator is introduced to reshape the input image of size  $m \times n \times c$  into four downsampled sub-images of size  $\frac{m}{2} \times \frac{n}{2} \times 4c$ . Here  $c$  is the number of channels, i.e.,  $c = 1$  for gray level image and  $c = 3$  for color image. In order to make learned CNN model insensitive to the bias between the input and ground truth noise levels and generate less artifacts, we propose to impose an orthogonal regularization on convolution filters, resulting in a robust FFDNet model.

#### A. Network Architecture

Fig. 1 illustrates the architecture of the proposed FFDNet. The first layer is a reversible downsampling operator which reshapes an  $m \times n$  noisy image  $\mathbf{y}$  into four downsampled sub-images. We further concatenate  $c$  tunable downsampled noise level maps  $\mathbf{m} = \{\mathbf{m}^1, \dots, \mathbf{m}^c\}$  with the downsampled sub-images to form a tensor  $\tilde{\mathbf{y}}$  of size  $\frac{m}{2} \times \frac{n}{2} \times 5c$  as the inputs to CNN. For spatially invariant AWGN with noise level  $\sigma$ ,  $\mathbf{m}$  is a uniform map with all elements being  $\sigma$ , and the downsampling will not lose any information. For spatially variant noise, it is natural to assume that the noise levels in a neighborhood change smoothly, and the use of downsampled  $\mathbf{m}$  is reasonable.

With the tensor  $\tilde{\mathbf{y}}$  as input, the following CNN consists of a series of  $3 \times 3$  convolutional layers. Each layer is composed of three types of operations: Convolution (Conv), Rectified Linear Units (ReLU) [31], and Batch Normalization (BN) [28]. More specifically, “Conv+ReLU” is adopted for the first convolutional layer, “Conv+BN+ReLU” for the middle layers, and “Conv” for the last convolutional layer. Zero-padding is employed to keep the size of feature maps unchanged after each convolution. After the last convolutional layer, an upscaling operation is applied as the reverse operator of the



downsampling operator applied in the input stage to produce the residual noisy image  $\tilde{\mathbf{n}}$  of size  $m \times n \times c$ . The denoised image is then obtained by  $\hat{\mathbf{x}} = \mathbf{y} - \tilde{\mathbf{n}}$ . Since FFDNet operates on downsampled sub-images, it is not necessary to employ the dilated convolution [29] to further increase the receptive field.

By considering the balance of complexity and performance, we set the number of convolutional layers as 15 for gray level image and 10 for color image. As to the number of feature maps, we set 64 for gray level image and 96 for color image. The reason that we use different settings for gray level and color images is twofold. First, since there are high dependencies among the R, G, B channels, using a smaller number convolutional layers is good enough to exploit the inter-channel dependency for denoising. Second, color image has more channels as input, and hence more feature (i.e., a larger number of feature maps) is required.

### B. Noise Level Map

Let's first revisit the model-based image denoising methods to analyze why they are flexible in handling noises at different levels, which will in turn help us to improve the flexibility of CNN-based denoiser. Most of the model-based denoising methods can be written as:

$$\hat{\mathbf{x}} = \arg \min_{\mathbf{x}} \frac{1}{2\sigma^2} \|\mathbf{y} - \mathbf{x}\|^2 + \lambda \Phi(\mathbf{x}), \quad (1)$$

where  $\frac{1}{2\sigma^2} \|\mathbf{y} - \mathbf{x}\|^2$  is the data fidelity term with noise level  $\sigma$ ,  $\Phi(\mathbf{x})$  is the regularization term associated with image prior, and  $\lambda$  controls the balance between the data fidelity and regularization terms. It is worth noting that in practice  $\lambda$  governs the compromise between noise reduction and details preservation. When it is too small, much noise will remain; on the opposite, details will be over-smoothed along with suppressing noise.

With some optimization algorithms, the solution of Eqn. (1) actually defines an implicit function  $\hat{\mathbf{x}} = f(\mathbf{y}, \sigma, \lambda)$  of the noisy image  $\mathbf{y}$ , noise level  $\sigma$ , and parameter  $\lambda$ . Since  $\lambda$  can be absorbed into  $\sigma$ , the solution  $\hat{\mathbf{x}} = f(\mathbf{y}, \sigma, \lambda)$  can be rewritten as  $\hat{\mathbf{x}} = f(\mathbf{y}, \sigma)$ . In this sense, setting noise level  $\sigma$  also plays the role of setting  $\lambda$  to control the tradeoff between noise reduction and details preservation. In a word, model-based methods are flexible in handling images with various noise levels by simply specifying  $\sigma$  in  $\hat{\mathbf{x}} = f(\mathbf{y}, \sigma)$ .

Model-based methods can also be extended to images with spatially variant noise by modifying the formulation as

$$\hat{\mathbf{x}} = \arg \min_{\mathbf{x}} \frac{1}{2} \sum_i ((\mathbf{y}_i - \mathbf{x}_i)/\sigma_i)^2 + \lambda \Phi(\mathbf{x}), \quad (2)$$

where  $\sigma_i$  denotes the noise level at location  $i$ ,  $\mathbf{y}_i$  and  $\mathbf{x}_i$  represent the pixel values of  $\mathbf{y}$  and  $\mathbf{x}$ , respectively. Let  $\mathbf{m}$  be the noise level map defined as  $\mathbf{m}_i = \sigma_i$ ,  $\sum_i ((\mathbf{y}_i - \mathbf{x}_i)/\sigma_i)^2$  can then be written as  $\|(\mathbf{y} - \mathbf{x}) \oslash \mathbf{m}\|^2$ , where  $\oslash$  denotes element-wise division. The optimization algorithm used to solve Eqn. (1) can be generalized to solve Eqn. (2), and the solution defines an implicit function  $\hat{\mathbf{x}} = f(\mathbf{y}, \mathbf{m})$  of the noisy image  $\mathbf{y}$  and noise level map  $\mathbf{m}$  for handling spatially variant noise.  $\mathbf{m}$  can have multiple channels to represent the noise level map of color images.

From the above discussion, one can see that model-based methods actually specify an implicit function  $\hat{\mathbf{x}} = f(\mathbf{y}, \mathbf{m})$ . Inspired by this fact, we propose to utilize CNN to learn an explicit mapping  $\hat{\mathbf{x}} = f(\mathbf{y}, \mathbf{m}; \Theta)$ . By taking the noisy image  $\mathbf{y}$  and the noise level map  $\mathbf{m}$  as the inputs, our proposed FFDNet model is expected to inherit the flexibility of model-based methods in handling images with different noise levels, even spatially variant noises.

### C. Denoising on Sub-images

Efficiency is another crucial issue for practical CNN-based denoising. One straightforward idea is to reduce the depth and number of filters. However, such a strategy will sacrifice much the modeling capacity and receptive field of CNN [20]. In [9], dilated convolution is introduced to expand receptive field without the increase of network depth, resulting in a 7-layer denoising CNN. Unfortunately, we empirically find that FFDNet with dilated convolution tends to generate artifacts around sharp edges.

Shi et al. [32] proposed to extract deep features directly from the low-resolution image for superresolution, and introduced a sub-pixel convolution layer to improve computational efficiency. In the application of image denoising, we introduce a reversible downsampling layer to reshape the input image into a set of small sub-images. Here the downsampling factor is set to 2 since it can largely improve the speed without reducing modeling capacity. The CNN is deployed on the sub-images, and finally a sub-pixel convolution layer is adopted to reverse the downsampling process.

Denoising on downsampled sub-images can also effectively expand the receptive field which in turn leads to a moderate network depth. For example, the proposed network with a depth of 15 and  $3 \times 3$  convolution will have a large receptive field of  $62 \times 62$ . In contrast, a plain 15-layer CNN only has a receptive field size of  $31 \times 31$ . We note that the receptive field of most state-of-the-art denoising methods ranges from  $35 \times 35$  to  $61 \times 61$  [20]. Further increase of receptive field actually benefits little in improving denoising performance [33]. What is more, the introduction of subsampling and sub-pixel convolution is effective in reducing the memory burden.

Experiments are conducted to validate the effectiveness of downsampling for balancing denoising accuracy and efficiency on the BSD68 dataset with  $\sigma = 15$  and 50. For gray level image denoising, we train a baseline CNN which has the same depth as FFDNet without downsampling. The comparison of average PSNR values is given as follows: (i) when  $\sigma$  is small (i.e., 15), the baseline CNN slightly outperforms FFDNet by 0.02dB; (ii) when  $\sigma$  is big (i.e., 50), FFDNet performs better than the baseline CNN by 0.09dB. However, FFDNet is nearly 3 times faster and is more memory-friendly than the baseline CNN. As a result, by performing denoising on sub-images, FFDNet significantly improves efficiency while maintaining denoising performance.

### D. Orthogonal Regularization on Convolution Filters

The inclusion of noise level map as inputs increases the difficulty of training. One key issue is how to make the

learned model still work well when the input noise level is less accurate. As shown in Fig. 2(a), when the input noise levels are accurate, the learned model can produce visually pleasant result. However, from Fig. 2(b), one can see that it may give rise to severe artifacts when the input noise level is much higher than the ground-truth one. In practice, we may deliberately over-estimate the noise level to remove as much as possible the noise. This requires the learned model to be robust to preserve the image main structures and details without introducing additional artifacts. Such a property is also useful in removing small structured noise in real noisy image (see Fig. 9(e)).

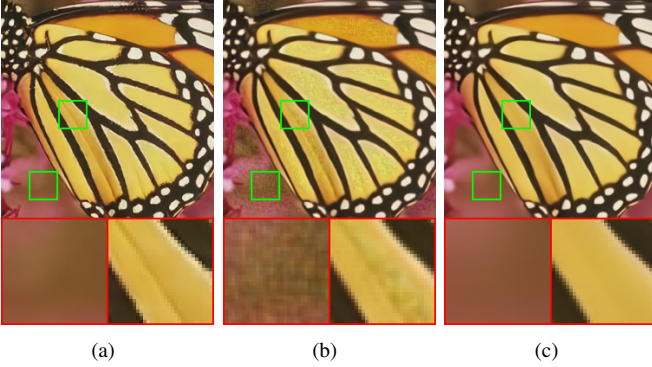


Fig. 2. An example to show the effectiveness of orthogonal regularization. The input is a noisy image with noise level 25. (a) Without orthogonal regularization but with matched noise level 25. (b) Without orthogonal regularization and with mismatched noise level 60. (c) With orthogonal regularization and mismatched noise level 60.

A simple solution to improve the robustness to noise level mismatch is to regularize the convolution filters. Here we resort to the orthogonal regularization, which aims to constrain the set of filters in an orthogonal space. Such a regularization is effective in eliminating the correlation between convolution filters, facilitating gradient propagation and improving the compactness of the learned model. Recent studies have demonstrated its advantages in enhancing the network generalization ability in applications of deep hashing and image classification [34], [35], [36], [37], [38].

We apply orthogonal regularization to FFDNet as follows. Suppose there are a set of  $3 \times 3$  convolution filters connecting input feature maps of  $C_{in}$  channels with output feature maps of  $C_{out}$  channels. We first reshape the filters into a two-dimensional matrix  $\mathbf{W}$  of size  $(3 \times 3 \times C_{in}) \times C_{out}$ . Then, singular value decomposition (SVD) is performed on  $\mathbf{W}$ , i.e.,  $\mathbf{W} = \mathbf{U}\mathbf{S}\mathbf{V}^T$ , where  $\mathbf{U}$  and  $\mathbf{V}$  are two orthogonal matrices and  $\mathbf{S}$  is a diagonal matrix of singular values. To enforce the orthogonality of  $\mathbf{W}$ , we simply replace all the singular values by 1. In the training stage, instead of performing SVD on each  $\mathbf{W}$  in each iteration, we perform SVD on each  $\mathbf{W}$  after every  $T$  iterations to reduce training time. Considering that orthogonal regularization may have adverse effect on performance [39], in our implementation the orthogonal regularization is first deployed and then abandoned when the learning rate becomes very small (i.e.,  $10^{-6}$ ). As can be seen in Fig. 2(c), orthogonal regularization is effective in suppressing unpleasant artifacts caused by noise level mismatch.

## IV. EXPERIMENTS

### A. Dataset Generation and Network Training

To train the FFDNet model, we need to prepare a training dataset of input-output pairs  $\{(\mathbf{y}_j, \mathbf{m}_j; \mathbf{x}_j)\}_{j=1}^N$ . Here,  $\mathbf{y}_j$  is obtained by adding AWGN to latent image  $\mathbf{x}_j$ , and  $\mathbf{m}_j$  is the noise level map. The reasons to use AWGN to generate the training dataset are as follows. First, AWGN is a natural choice when there is no specific prior information on noise source. Second, real-world noise can be approximated as locally AWGN [40]. Moreover, due to the use of orthogonal regularization, FFDNet is robust to the mismatch of input noise level, and performs well for real noise which violates the AWGN assumption. Taking these into account, we employ synthetic AWGN to generate noisy data to train FFDNet. More specifically, FFDNet model is trained on the noisy images  $\mathbf{y}_j = \mathbf{x}_j + \mathbf{n}_j$  without quantization to 8-bit integer values. Though the real noisy images are generally 8-bit quantized, we empirically found that the learned model still works effectively on real noisy images.

To generate training image pairs, we collected a large dataset of source images, including 400 BSD images, 400 images selected from the validation set of ImageNet [41], and the 4,744 images from the Waterloo Exploration Database [42]. We crop patches from these images and use  $N = 128 \times 8,000$  patches for training. The patch size should be larger than the receptive field of FFDNet, and we set it to  $65 \times 65$  and  $45 \times 45$  for gray level images and color images, respectively. The noisy patches are obtained by adding AWGN of noise level  $\sigma \in [0, 75]$  (or  $[\sigma_R, \sigma_G, \sigma_B]$  for each of the R, G, B channels of color images) to the clean patches. The ADAM algorithm [43] is adopted to optimize FFDNet by minimizing the following loss function,

$$\ell(\Theta) = \frac{1}{2N} \sum_{j=1}^N \|f(\mathbf{y}_j, \mathbf{m}_j; \Theta) - \mathbf{x}_j\|_F^2 \quad (3)$$

The learning rate starts from  $10^{-3}$  and reduces to  $10^{-4}$  when the training error stops decreasing. When the training error keeps unchanged in five sequential epochs, we abandon the orthogonal regularization and merge the parameters of each batch normalization into the adjacent convolution filters. Then, a smaller learning rate of  $10^{-6}$  is adopted for additional 20 epochs to fine-tune the FFDNet model. As for the other hyper-parameters of ADAM, we use their default settings. The mini-batch size is set as 128, and the rotation and flip based data augmentation is also adopted during training. The FFDNet models are trained in Matlab (R2015b) environment with MatConvNet package [44] and an Nvidia Titan X Pascal GPU. The training of a single model can be done in about one day.

To evaluate the proposed FFDNet denoisers on gray level image denoising, we use two datasets, i.e., BSD68 [3] and Set12, to test FFDNet for removing AWGN noise, and use the ‘‘RNI6’’ dataset [45] to test FFDNet for removing real noise. The BSD68 dataset consists of 68 images from the separate test set of the BSD dataset. The Set12 dataset is a collection of widely-used testing images. The RNI6 dataset contains 6 real noisy images without ground truth.

As for color image denoising, we employ four datasets, namely CBSD68, Kodak24 [46], McMaster [47], and “RNI15” [45], [48]. The CBSD68 dataset is the corresponding color version of the gray level BSD68 dataset. The Kodak24 dataset consists of 24 center-cropped images of size  $500 \times 500$  from the original Kodak dataset. The McMaster dataset is a widely-used dataset for color demosaicing, which contains 18 cropped images of size  $500 \times 500$ . Compared to the Kodak24 images, the images in McMaster dataset exhibit more saturated colors [47]. The RNI15 dataset consists of 15 real noisy images. We note that RNI6 and RNI15 cover a variety of real noise types, such as camera noise and JPEG compression noise. Since the ground truth clean images are unavailable for real noisy images, we thus only provide the visual comparisons on these images. The testing code of our FFDNet models can be downloaded at <https://github.com/csxn/FFDNet>.

### B. Experiments on AWGN Removal

In this subsection, we test FFDNet on noisy images corrupted by spatially invariant AWGN. For gray level image denoising, we compare FFDNet with state-of-the-art methods BM3D [11], WNNM [5], MLP [18], TNRD [17], and DnCNN [20]. Note that BM3D and WNNM are two representative model-based methods based on nonlocal self-similarity prior, whereas TNRD, MLP and DnCNN are discriminative learning based methods. Tables I and II report the PSNR results on BSD68 and Set12 datasets, respectively. From Tables I and II, one can have the following observations.

First, FFDNet surpasses BM3D by a large margin and outperforms WNNM, MLP and TNRD by about 0.2dB for a wide range of noise levels on BSD68. Second, FFDNet is slightly inferior to DnCNN when the noise level is low (e.g.,  $\sigma \leq 25$ ), but gradually outperforms DnCNN with the increase of noise level (e.g.,  $\sigma > 25$ ). This phenomenon may be resulted from the tradeoff between receptive field size and modeling capacity. FFDNet has a larger receptive field than DnCNN, thus favoring for removing strong noise, while DnCNN has better modeling capacity which is beneficial for denoising images with lower noise level. Third, FFDNet outperforms WNNM on images such as “House”, while it is inferior to WNNM on image “Barbara”. This is because “Barbara” has a rich amount of repetitive structures, which can be effectively exploited by nonlocal self-similarity based WNNM method. The visual comparisons of different methods are given in Fig. 3. Overall, FFDNet produces the best perceptual quality of denoised images.

For color image denoising, we compare FFDNet with the CBM3D method [11]. Table III reports the performance of CBM3D and FFDNet on CBSD68, Kodak24, and McMaster datasets, and Figs. 4 and 5 present the visual comparisons. It can be seen that FFDNet consistently outperforms CBM3D on different noise levels in terms of both quantitative and qualitative evaluation.

### C. Experiments on Spatially Variant AWGN Removal

We then test the flexibility of FFDNet to deal with spatially variant AWGN. To synthesize spatially variant AWGN, we

first generate an AWGN image  $\mathbf{n}_1$  with unit standard deviation and a noise level map  $\mathbf{m}$  of the same size. Then, element-wise multiplication is applied on  $\mathbf{n}_1$  and  $\mathbf{m}$  to produce the spatially variant AWGN, i.e.,  $\mathbf{n} = \mathbf{n}_1 \odot \mathbf{m}$ . In the denoising stage, we take the bilinearly downsampled noise level map as the input to FFDNet. Since the noise level map is spatially smooth, the use of downsampled noise level map generally has very little effect on the final denoising performance.

Fig. 6 shows the denoising results of FFDNet for four spatially variant AWGN. We do not compare FFDNet with other methods because no state-of-the-art AWGN denoising method can be readily extended to handle spatially variant AWGN. From Fig. 6, one can see that FFDNet is flexible and powerful to remove spatially variant AWGN. Even when the R, G, B channels are corrupted by different types of spatially variant AWGN, visually pleasant result can still be obtained by FFDNet.

### D. Experiments on Noise Level Sensitivity

In practical applications, the noise level map may not be accurately estimated from the noisy observation, and mismatch between the input and real noise levels is inevitable. If the input noise level is lower than the real noise level, the noise cannot be completely removed. Therefore, users often prefer to set a higher noise level to remove more noise. However, this may also remove too much image details together with noise. A practical denoiser should tolerate certain mismatch of noise levels. In this subsection, we evaluate FFDNet in comparison with benchmark BM3D and DnCNN by varying different input noise levels for a given ground truth noise level.

Fig. 7 illustrates the noise level sensitivity curves of BM3D, DnCNN and FFDNet. Different methods with different input noise levels (e.g., “FFDNet-15” represents FFDNet with input noise level fixed as 15) are evaluated on BSD68 images with noise level ranging from 0 to 50. Fig. 8 shows the visual comparisons between BM3D/CBM3D and FFDNet by setting different input noise levels to denoise a noisy image. Four typical image structures, including flat region, sharp edge, line with high contrast, and line with low contrast, are selected for visual comparison to investigate the noise level sensitivity of BM3D and FFDNet. From Figs. 7 and 8, we have the following observations.

- On all noise levels, FFDNet achieves similar denoising results to BM3D and DnCNN when their input noise levels are the same.
- With the fixed input noise level, for all the three methods, the PSNR value tends to stay the same when the ground truth noise level is lower, and begins to decrease when the ground truth noise level is higher.
- The best visual quality is obtained when the input noise level matches the ground truth one. BM3D and FFDNet produce similar visual results with lower input noise levels, while they exhibit certain difference with higher input noise levels. Both of them will smooth out noise in flat regions, and gradually smooth image structures with the increase of input noise levels. Particularly, FFDNet may wipe out some low contrast line structure, whereas



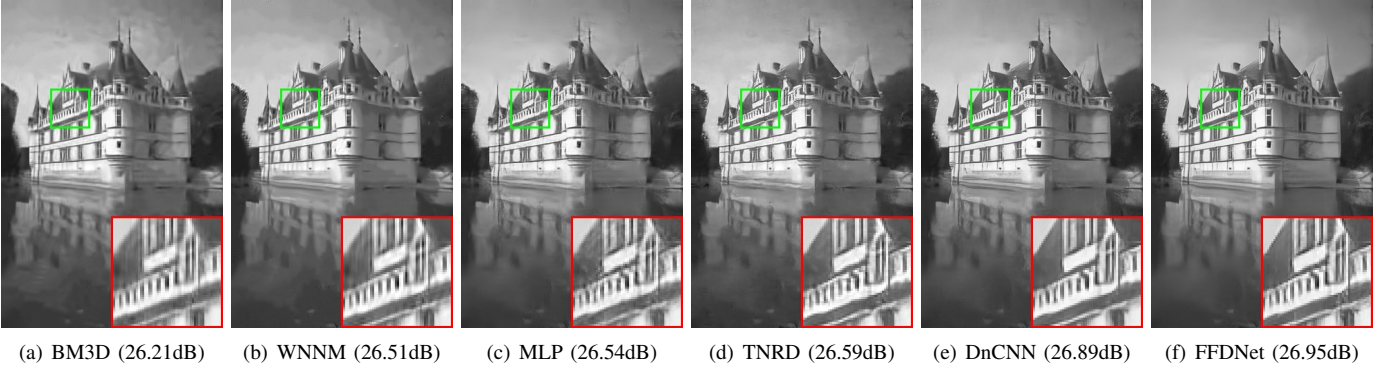


Fig. 3. Denoising results on image “102061” from the BSD68 dataset with noise level 50 by different methods.

TABLE I  
THE PSNR(DB) RESULTS OF DIFFERENT METHODS ON SET12 DATASET WITH NOISE LEVELS 15, 25 35, 50 AND 75. THE BEST TWO RESULTS ARE HIGHLIGHTED IN RED AND BLUE COLORS, RESPECTIVELY.

| Images      | <i>C.man</i>  | <i>House</i> | <i>Peppers</i> | <i>Starfish</i> | <i>Monarch</i> | <i>Airplane</i> | <i>Parrot</i> | <i>Lena</i>  | <i>Barbara</i> | <i>Boat</i>  | <i>Man</i>   | <i>Couple</i> | <i>Average</i> |
|-------------|---------------|--------------|----------------|-----------------|----------------|-----------------|---------------|--------------|----------------|--------------|--------------|---------------|----------------|
| Noise Level | $\sigma = 15$ |              |                |                 |                |                 |               |              |                |              |              |               |                |
| BM3D        | 31.91         | 34.93        | 32.69          | 31.14           | 31.85          | 31.07           | 31.37         | 34.26        | <b>33.10</b>   | 32.13        | 31.92        | 32.10         | 32.37          |
| WNNM        | 32.17         | <b>35.13</b> | 32.99          | 31.82           | <b>32.71</b>   | 31.39           | 31.62         | 34.27        | <b>33.60</b>   | 32.27        | 32.11        | 32.17         | 32.70          |
| TNRD        | 32.19         | 34.53        | 33.04          | 31.75           | 32.56          | 31.46           | 31.63         | 34.24        | 32.13          | 32.14        | 32.23        | 32.11         | 32.50          |
| DnCNN       | <b>32.61</b>  | 34.97        | <b>33.30</b>   | <b>32.20</b>    | <b>33.09</b>   | <b>31.70</b>    | <b>31.83</b>  | <b>34.62</b> | 32.64          | <b>32.42</b> | <b>32.46</b> | <b>32.47</b>  | <b>32.86</b>   |
| FFDNet      | <b>32.43</b>  | <b>35.07</b> | <b>33.25</b>   | <b>31.99</b>    | 32.66          | <b>31.57</b>    | <b>31.81</b>  | <b>34.62</b> | 32.54          | <b>32.38</b> | <b>32.41</b> | <b>32.46</b>  | <b>32.77</b>   |
| Noise Level | $\sigma = 25$ |              |                |                 |                |                 |               |              |                |              |              |               |                |
| BM3D        | 29.45         | 32.85        | 30.16          | 28.56           | 29.25          | 28.42           | 28.93         | 32.07        | <b>30.71</b>   | 29.90        | 29.61        | 29.71         | 29.97          |
| WNNM        | 29.64         | <b>33.22</b> | 30.42          | 29.03           | 29.84          | 28.69           | 29.15         | 32.24        | <b>31.24</b>   | 30.03        | 29.76        | 29.82         | 30.26          |
| MLP         | 29.61         | 32.56        | 30.30          | 28.82           | 29.61          | 28.82           | 29.25         | 32.25        | 29.54          | 29.97        | 29.88        | 29.73         | 30.03          |
| TNRD        | 29.72         | 32.53        | 30.57          | 29.02           | 29.85          | 28.88           | 29.18         | 32.00        | 29.41          | 29.91        | 29.87        | 29.71         | 30.06          |
| DnCNN       | <b>30.18</b>  | 33.06        | <b>30.87</b>   | <b>29.41</b>    | <b>30.28</b>   | <b>29.13</b>    | <b>29.43</b>  | <b>32.44</b> | 30.00          | <b>30.21</b> | <b>30.10</b> | <b>30.12</b>  | <b>30.43</b>   |
| FFDNet      | <b>30.10</b>  | <b>33.28</b> | <b>30.93</b>   | <b>29.32</b>    | <b>30.08</b>   | <b>29.04</b>    | <b>29.44</b>  | <b>32.57</b> | 30.01          | <b>30.25</b> | <b>30.11</b> | <b>30.20</b>  | <b>30.44</b>   |
| Noise Level | $\sigma = 35$ |              |                |                 |                |                 |               |              |                |              |              |               |                |
| BM3D        | 27.92         | 31.36        | 28.51          | 26.86           | 27.58          | 26.83           | 27.40         | 30.56        | <b>28.98</b>   | 28.43        | 28.22        | 28.15         | 28.40          |
| WNNM        | 28.08         | <b>31.92</b> | 28.75          | 27.27           | 28.13          | 27.10           | 27.69         | 30.73        | <b>29.48</b>   | 28.54        | 28.33        | 28.24         | 28.69          |
| MLP         | 28.08         | 31.18        | 28.54          | 27.12           | 27.97          | 27.22           | 27.72         | 30.82        | 27.62          | 28.53        | 28.47        | 28.24         | 28.46          |
| DnCNN       | <b>28.61</b>  | 31.61        | <b>29.14</b>   | <b>27.53</b>    | <b>28.51</b>   | <b>27.52</b>    | <b>27.94</b>  | <b>30.91</b> | 28.09          | <b>28.72</b> | <b>28.66</b> | <b>28.52</b>  | <b>28.82</b>   |
| FFDNet      | <b>28.57</b>  | <b>31.96</b> | <b>29.32</b>   | <b>27.57</b>    | <b>28.49</b>   | <b>27.46</b>    | <b>28.02</b>  | <b>31.16</b> | 28.30          | <b>28.83</b> | <b>28.71</b> | <b>28.70</b>  | <b>28.92</b>   |
| Noise Level | $\sigma = 50$ |              |                |                 |                |                 |               |              |                |              |              |               |                |
| BM3D        | 26.13         | 29.69        | 26.68          | 25.04           | 25.82          | 25.10           | 25.90         | 29.05        | <b>27.22</b>   | 26.78        | 26.81        | 26.46         | 26.72          |
| WNNM        | 26.45         | <b>30.33</b> | 26.95          | 25.44           | 26.32          | 25.42           | 26.14         | 29.25        | <b>27.79</b>   | 26.97        | 26.94        | 26.64         | 27.05          |
| MLP         | 26.37         | 29.64        | 26.68          | 25.43           | 26.26          | 25.56           | 26.12         | 29.32        | 25.24          | 27.03        | 27.06        | 26.67         | 26.78          |
| TNRD        | 26.62         | 29.48        | 27.10          | 25.42           | 26.31          | 25.59           | 26.16         | 28.93        | 25.70          | 26.94        | 26.98        | 26.50         | 26.81          |
| DnCNN       | <b>27.03</b>  | 30.00        | <b>27.32</b>   | <b>25.70</b>    | <b>26.78</b>   | <b>25.87</b>    | <b>26.48</b>  | <b>29.39</b> | 26.22          | <b>27.20</b> | <b>27.24</b> | <b>26.90</b>  | <b>27.18</b>   |
| FFDNet      | <b>27.05</b>  | <b>30.37</b> | <b>27.54</b>   | <b>25.75</b>    | <b>26.81</b>   | <b>25.89</b>    | <b>26.57</b>  | <b>29.66</b> | 26.45          | <b>27.33</b> | <b>27.29</b> | <b>27.08</b>  | <b>27.32</b>   |
| Noise Level | $\sigma = 75$ |              |                |                 |                |                 |               |              |                |              |              |               |                |
| BM3D        | 24.32         | 27.51        | 24.73          | 23.27           | 23.91          | 23.48           | 24.18         | 27.25        | <b>25.12</b>   | 25.12        | 25.32        | 24.70         | 24.91          |
| WNNM        | 24.60         | <b>28.24</b> | 24.96          | 23.49           | 24.31          | 23.74           | 24.43         | 27.54        | <b>25.81</b>   | 25.29        | 25.42        | 24.86         | <b>25.23</b>   |
| MLP         | 24.63         | 27.78        | 24.88          | 23.57           | 24.40          | 23.87           | 24.55         | <b>27.68</b> | 23.39          | 25.44        | 25.59        | <b>25.02</b>  | 25.07          |
| DnCNN       | <b>25.07</b>  | 27.85        | <b>25.17</b>   | <b>23.64</b>    | <b>24.71</b>   | <b>24.03</b>    | <b>24.71</b>  | 27.54        | 23.63          | <b>25.47</b> | <b>25.64</b> | 24.97         | 25.20          |
| FFDNet      | <b>25.34</b>  | <b>28.37</b> | <b>25.53</b>   | <b>23.79</b>    | <b>24.88</b>   | <b>24.17</b>    | <b>24.94</b>  | <b>27.93</b> | 24.27          | <b>25.65</b> | <b>25.73</b> | <b>25.29</b>  | <b>25.49</b>   |

TABLE II  
THE AVERAGE PSNR(DB) RESULTS OF DIFFERENT METHODS ON BSD68 WITH NOISE LEVELS 15, 25 35, 50 AND 75.

| Methods       | BM3D  | WNNM  | MLP   | TNRD  | DnCNN | FFDNet |
|---------------|-------|-------|-------|-------|-------|--------|
| $\sigma = 15$ | 31.07 | 31.37 | —     | 31.42 | 31.72 | 31.62  |
| $\sigma = 25$ | 28.57 | 28.83 | 28.96 | 28.92 | 29.23 | 29.19  |
| $\sigma = 35$ | 27.08 | 27.30 | 27.50 | —     | 27.69 | 27.73  |
| $\sigma = 50$ | 25.62 | 25.87 | 26.03 | 25.97 | 26.23 | 26.30  |
| $\sigma = 75$ | 24.21 | 24.40 | 24.59 | —     | 24.64 | 24.78  |

BM3D can still preserve the mean patch regardless of the input noise levels due to its use of nonlocal information.

- Using a higher input noise level can generally produce better visual results than using a lower one. In addition, there is no much visual difference when the input noise level is a little higher than the ground truth one.

According to above observations, FFDNet exhibits similar noise level sensitivity performance to BM3D and DnCNN in balancing noise reduction and details preservation. When the ground truth noise level is unknown, it is more preferable to

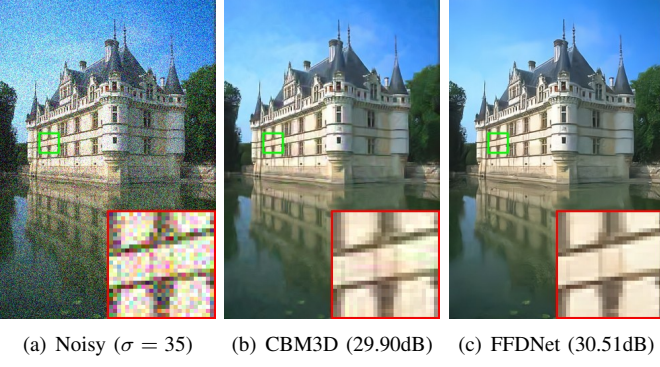


Fig. 4. Color image denoising results by CBM3D and FFDNet.

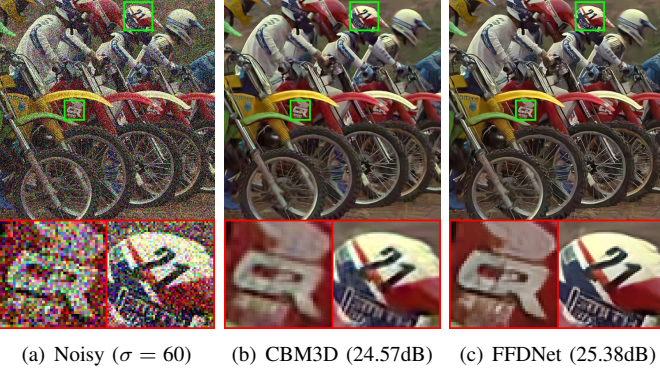


Fig. 5. Color image denoising results by CBM3D and FFDNet.

TABLE III  
THE AVERAGE PSNR(DB) RESULTS OF CBM3D AND FFDNet ON CBSD68, KODAK24 AND MCMaster DATASETS WITH NOISE LEVELS 15, 25 35, 50 AND 75.

| Datasets | Methods | $\sigma=15$ | $\sigma=25$ | $\sigma=35$ | $\sigma=50$ | $\sigma=75$ |
|----------|---------|-------------|-------------|-------------|-------------|-------------|
| CBSD68   | CBM3D   | 33.52       | 30.71       | 28.89       | 27.38       | 25.74       |
|          | FFDNet  | 33.80       | 31.18       | 29.57       | 27.96       | 26.24       |
| Kodak24  | CBM3D   | 34.28       | 31.68       | 29.90       | 28.46       | 26.82       |
|          | FFDNet  | 34.55       | 32.11       | 30.56       | 28.99       | 27.25       |
| McMaster | CBM3D   | 34.06       | 31.66       | 29.92       | 28.51       | 26.79       |
|          | FFDNet  | 34.47       | 32.25       | 30.76       | 29.14       | 27.29       |

set a larger input noise level than a lower one to remove noise with better perceptual quality.

#### E. Experiments on Real Noisy Images

In this subsection, real noisy images are used to further assess the practicability of FFDNet. However, such an evaluation is difficult to conduct due to the following reasons. (i) Both the ground truth clean image and noise level are unknown for real noisy image. (ii) The real noise comes from various sources such as camera pipeline (e.g., shot noise, amplifier noise and quantization noise), scanning, lossy compression and image resizing [49], [50], and it is generally non-Gaussian, spatially variant, and signal-dependent. As a result, the AWGN assumption in many denoising algorithms does not hold, and the associated noise level estimation methods do not work well for real noisy images.

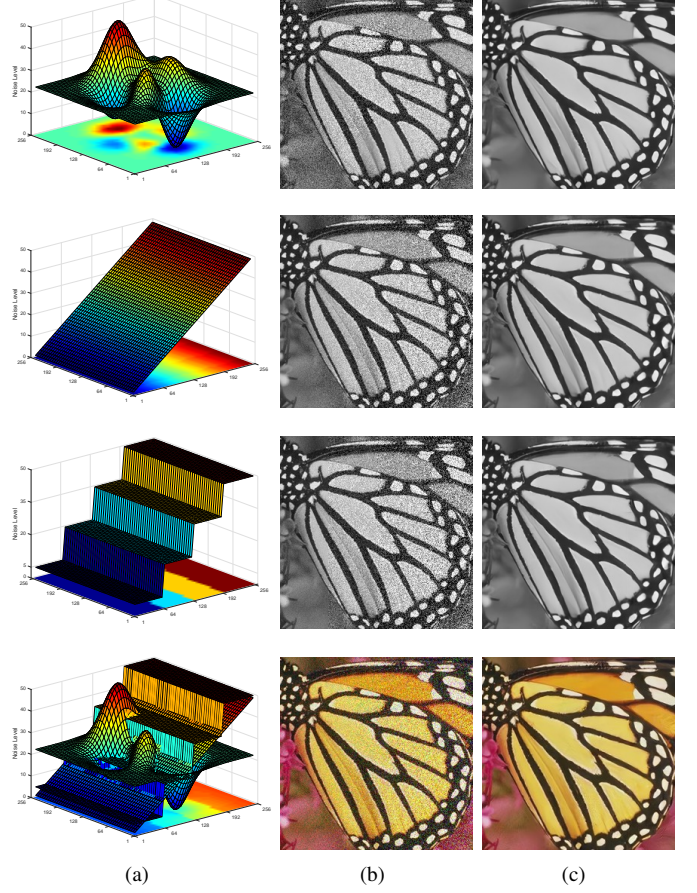


Fig. 6. Examples of FFDNet on removing spatially variant AWGN. Left column: noise level maps. Middle column, from top to bottom: noisy images with PSNR 20.55dB, 19.42dB, 18.62dB and 19.66dB. Right column, from top to bottom: denoised images (PSNR: 29.97dB, 29.40dB, 28.94dB and 30.55dB) by FFDNet.

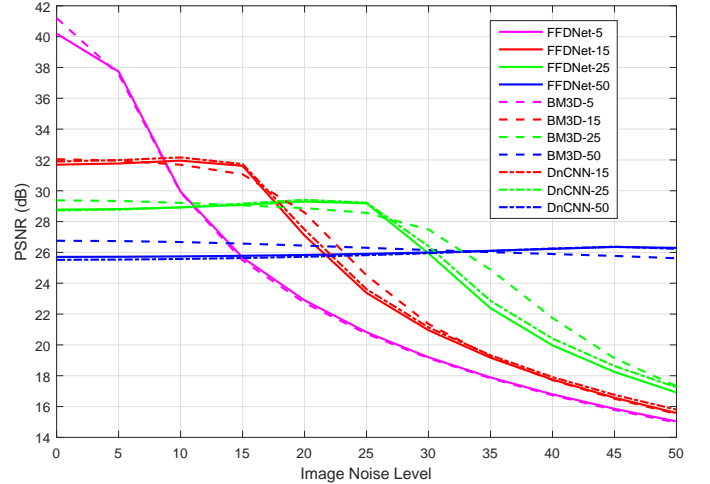


Fig. 7. Noise level sensitivity curves of BM3D, DnCNN and FFDNet. The averaged PSNR results are evaluated on BSD68.

Instead of adopting any noise level estimation methods, we adopt an interactive strategy to handle real noisy images. First of all, we empirically found that the assumption of spatially invariant noise usually works well for most real noisy



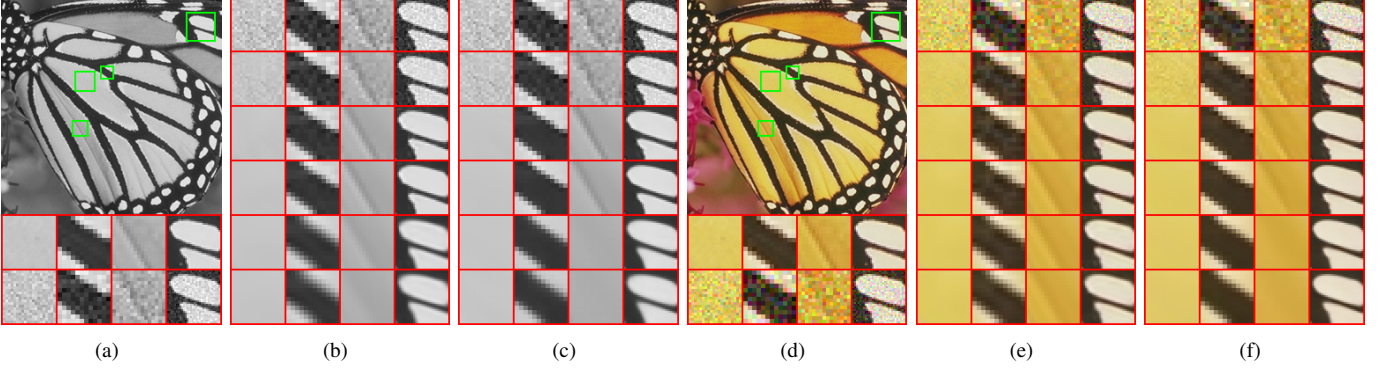


Fig. 8. Visual comparisons between FFDNet and BM3D/CBM3D by setting different input noise levels to denoise a noisy image. (a) From top to bottom: ground truth image, four clean zoom-in regions, and the corresponding noisy regions (AWGN, noise level 15). (b) From top to bottom: denoising results by BM3D with input noise levels 5, 10, 15, 20, 50, and 75, respectively. (c) Results by FFDNet with the same settings as in (b). (d) From top to bottom: ground truth image, four clean zoom-in regions, and the corresponding noisy regions (AWGN, noise level 25). (e) From top to bottom: denoising results by CBM3D with input noise levels 10, 20, 25, 30, 45 and 60, respectively. (f) Results by FFDNet with the same settings as in (e).

images. We then employ a set of typical input noise levels to produce multiple outputs, and select the one which has best tradeoff between noise reduction and details preservation. Second, for spatially variant noise, we sample several typical image patches which represent the distinct regions of different noise levels and apply different input noise levels to them. By observing the denoising results, we then choose the proper noise level for each typical patch. The noise levels at other locations are interpolated from the noise levels of the typical patches. An approximation of non-uniform noise level map can then be obtained. In our following experiments, unless otherwise specified, we assume spatially invariant noise for the real noisy images.

Since there is no ground-truth image for a real noisy image, visual comparison is employed to evaluate the performance of FFDNet. We choose BM3D for comparison because it is widely accepted as a benchmark for denoising applications. Given a noisy image, the same input noise level is used for BM3D and FFDNet. A blind denoising algorithm, the Noise Clinic [45] method, is also employed for comparison. Fig. 9 compares the gray level image denoising results of Noise Clinic, BM3D and FFDNet on RNI6 images. As one can see, Noise Clinic reduces much the noise but it also generates many algorithm-induced artifacts. BM3D and FFDNet produce more visually pleasant results. In particular, there are some structured noise in image “Building”. Noise Clinic and BM3D fail to remove those structured noises, because the structured noises fit the nonlocal self-similarity prior adopted in Noise Clinic and BM3D. FFDNet removes such noise without losing underlying image textures. This is because FFDNet learns the image priors from large scale training data and can correctly distinguish structured noise from image details.

Fig. 10 shows the denoising results of Noise Clinic, CBM3D and FFDNet on five color noisy images from RNI15. The three competing methods exhibit similar behaviors to those on denoising gray level images. From the denoising results of “Pattern1” and “Boy”, one can see that CBM3D remains the structured color noise unremoved whereas FFDNet removes successfully such kind of noise. We can conclude that while

the nonlocal self-similarity prior helps to remove random noise, it hinders the removal of structured noise. In comparison, the prior implicitly learned by CNN is able to remove both random noise and structured noise. Fig. 11 further shows more visual results of FFDNet on the other nine images from RNI15. It can be seen that FFDNet can handle various kinds of noises, including Gaussian-like noise (see image “Frog”), JPEG lossy compression noise (see image “Audrey Hepburn”), and video noise (see image “Movie”).

Fig. 12 shows a more challenging example to demonstrate the advantage of FFDNet for denoising noisy images with spatially variant noise. As one can see, while FFDNet with a small input noise level can recover the details of regions with low noise level, it fails to remove strong noise. On the other hand, FFDNet with a large input noise level can remove strong noise but it will also smooth out the details in the region with low noise level. In contrast, the denoising result with a proper non-uniform noise level map not only preserves image details but also removes the strong noise.

Finally, according to the above experiments on real noisy images, we can see that the FFDNet model trained with unquantized image data performs well on 8-bit quantized real noisy images.

#### F. Running Time

Table IV lists the running time results of BM3D, DnCNN and FFDNet for denoising gray level and color images with size  $256 \times 256$ ,  $512 \times 512$  and  $1024 \times 1024$ . The evaluation was performed in Matlab (R2015b) environment on a computer with a six-core Intel(R) Core(TM) i7-5820K CPU @ 3.3GHz, 32 GB of RAM and an Nvidia Titan X Pascal GPU. For BM3D, we evaluate its running time by denoising images with noise level 25. For DnCNN, the gray level and color image denoising models have 17 and 20 convolutional layers, respectively. The Nvidia cuDNN-v5.1 deep learning library is used to accelerate the computation of DnCNN and FFDNet. The memory transfer time between CPU and GPU is also counted. Note that DnCNN and FFDNet can be implemented with both single-threaded (ST) and multi-threaded (MT) CPU computations.



Fig. 9. Gray level image denoising results by different methods on real noisy images. From top to bottom: noisy images, denoised images by Noise Clinic, denoised images by BM3D, denoised images by FFDNet. (a)  $\sigma = 14$ ; (b)  $\sigma = 15$ ; (c)  $\sigma = 10$ ; (d)  $\sigma = 20$ ; (e)  $\sigma = 20$ ; (f)  $\sigma = 7$ .

TABLE IV  
RUNNING TIME (IN SECONDS) OF DIFFERENT METHODS FOR DENOISING  
IMAGES WITH SIZE  $256 \times 256$ ,  $512 \times 512$  AND  $1024 \times 1024$ .

| Methods | Device  | $256 \times 256$ |       | $512 \times 512$ |       | $1024 \times 1024$ |       |
|---------|---------|------------------|-------|------------------|-------|--------------------|-------|
|         |         | Gray             | Color | Gray             | Color | Gray               | Color |
| BM3D    | CPU(ST) | 0.59             | 0.98  | 2.52             | 3.57  | 10.77              | 20.15 |
| DnCNN   | CPU(ST) | 2.14             | 2.44  | 8.63             | 9.85  | 32.82              | 38.11 |
|         | CPU(MT) | 0.74             | 0.98  | 3.41             | 4.10  | 12.10              | 15.48 |
|         | GPU     | 0.011            | 0.014 | 0.033            | 0.040 | 0.124              | 0.167 |
| FFDNet  | CPU(ST) | 0.44             | 0.52  | 1.81             | 2.14  | 7.24               | 8.51  |
|         | CPU(MT) | 0.18             | 0.19  | 0.73             | 0.79  | 2.96               | 3.15  |
|         | GPU     | 0.006            | 0.007 | 0.012            | 0.016 | 0.038              | 0.054 |

From Table IV, we have the following observations. First, BM3D spends much more time on denoising color images than gray level images. The reason is that, compared to gray-BM3D, CBM3D needs extra time to denoise the chrominance components after luminance-chrominance color transformation. Second, while DnCNN can benefit from GPU compu-

tation for fast implementation, it has comparable CPU time to BM3D. Third, FFDNet spends almost the same time for processing gray level and color images. More specifically, FFDNet with multi-threaded implementation is about three times faster than DnCNN and BM3D on CPU, and much faster than DnCNN on GPU. Even with single-threaded implementation, FFDNet is also faster than BM3D. Taking denoising performance and flexibility into consideration, FFDNet is very competitive for practical applications.

## V. CONCLUSION

In this paper, we proposed a new CNN model, namely FFDNet, for fast, effective and flexible discriminative denoising. To achieve this goal, several techniques were utilized in network design and training, including the use of noise level map as input, denoising in downsampled sub-images space, and imposing orthogonal regularization on convolution filters. The results on synthetic images with AWGN demonstrated



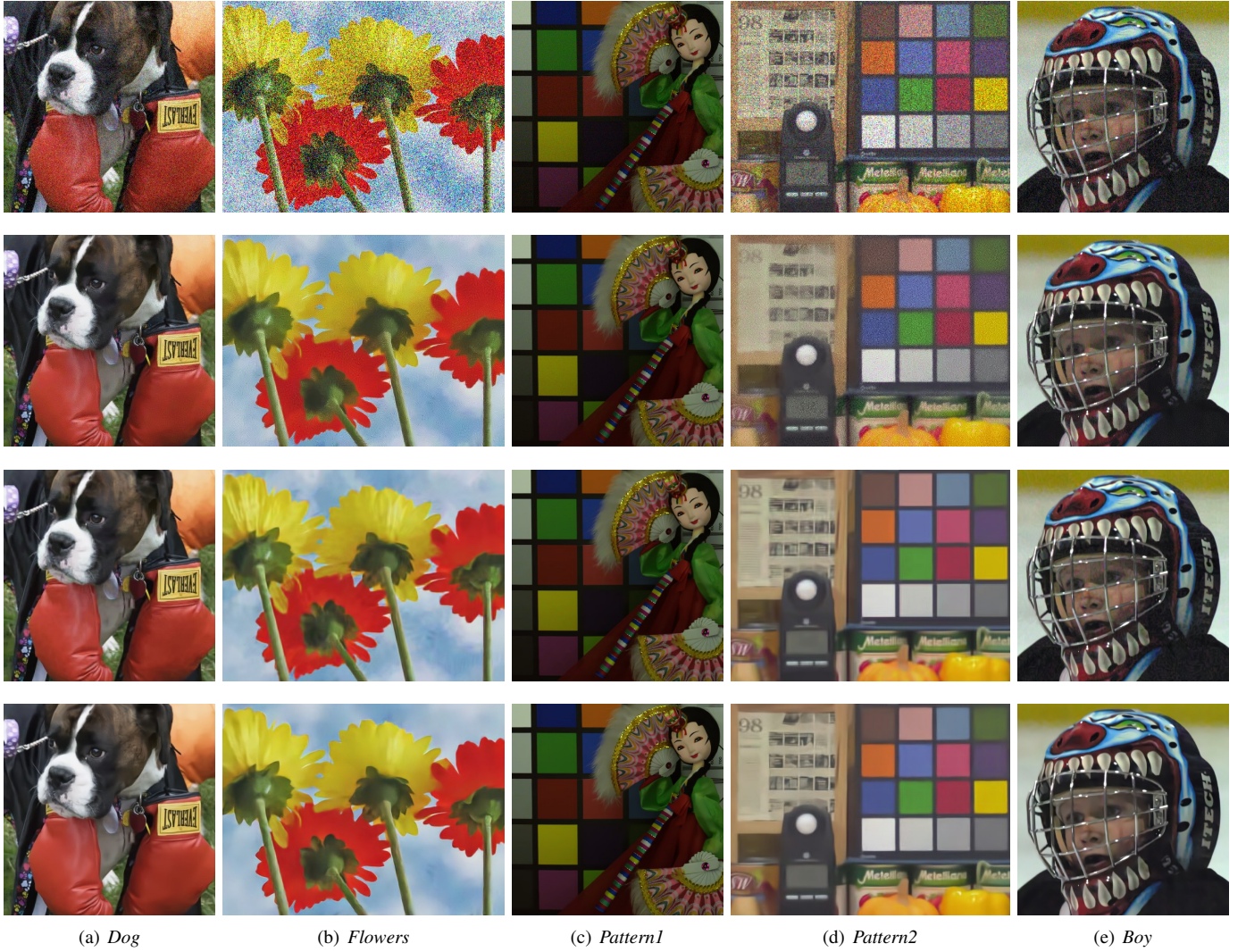


Fig. 10. Color image denoising results by different methods on real noisy images. From top to bottom: noisy images, denoised images by Noise Clinic, denoised images by CBM3D, denoised images by FFDNet. (a)  $\sigma = 28$ ; (b)  $\sigma = 70$ ; (c)  $\sigma = 12$ ; (d)  $\sigma = 45$ ; (e)  $\sigma = 45$ .

that FFDNet can not only produce state-of-the-art results when input noise level matches ground truth noise level, but also have good robustness to the mismatch of input noise levels. The results on images with spatially variant AWGN validated the flexibility of FFDNet for handling inhomogeneous noise. The results on real noisy images further demonstrated that FFDNet can deliver perceptually appealing denoising results. Finally, the running time comparisons showed the faster speed of FFDNet over other competing methods such as BM3D. Considering its flexibility, efficiency and effectiveness, FFDNet provides a practical solution to CNN denoising applications.

## REFERENCES

- [1] H. C. Andrews and B. R. Hunt, "Digital image restoration," *Prentice-Hall Signal Processing Series*, Englewood Cliffs: Prentice-Hall, 1977, vol. 1, 1977.
- [2] P. Chatterjee and P. Milanfar, "Is denoising dead?" *IEEE Transactions on Image Processing*, vol. 19, no. 4, pp. 895–911, 2010.
- [3] S. Roth and M. J. Black, "Fields of experts: A framework for learning image priors," in *IEEE Computer Society Conference on Computer Vision and Pattern Recognition*, vol. 2, 2005, pp. 860–867.
- [4] D. Zoran and Y. Weiss, "From learning models of natural image patches to whole image restoration," in *IEEE International Conference on Computer Vision*, 2011, pp. 479–486.
- [5] S. Gu, L. Zhang, W. Zuo, and X. Feng, "Weighted nuclear norm minimization with application to image denoising," in *IEEE Conference on Computer Vision and Pattern Recognition*, 2014, pp. 2862–2869.
- [6] M. V. Afonso, J. M. Bioucas-Dias, and M. A. Figueiredo, "Fast image recovery using variable splitting and constrained optimization," *IEEE Transactions on Image Processing*, vol. 19, no. 9, pp. 2345–2356, 2010.
- [7] F. Heide, M. Steinberger, Y.-T. Tsai, M. Rouf, D. Pajak, D. Reddy, O. Gallo, J. Liu, W. Heidrich, K. Egiazarian *et al.*, "FlexISP: A flexible camera image processing framework," *ACM Transactions on Graphics*, vol. 33, no. 6, p. 231, 2014.
- [8] Y. Romano, M. Elad, and P. Milanfar, "The little engine that could: Regularization by denoising (RED)," *submitted to SIAM Journal on Imaging Sciences*, 2016.
- [9] K. Zhang, W. Zuo, S. Gu, and L. Zhang, "Learning deep CNN denoiser prior for image restoration," in *IEEE Conference on Computer Vision and Pattern Recognition*, 2017, pp. 3929–3938.
- [10] J. Portilla, V. Strela, M. J. Wainwright, and E. P. Simoncelli, "Image denoising using scale mixtures of gaussians in the wavelet domain," *IEEE Transactions on Image processing*, vol. 12, no. 11, pp. 1338–1351, 2003.



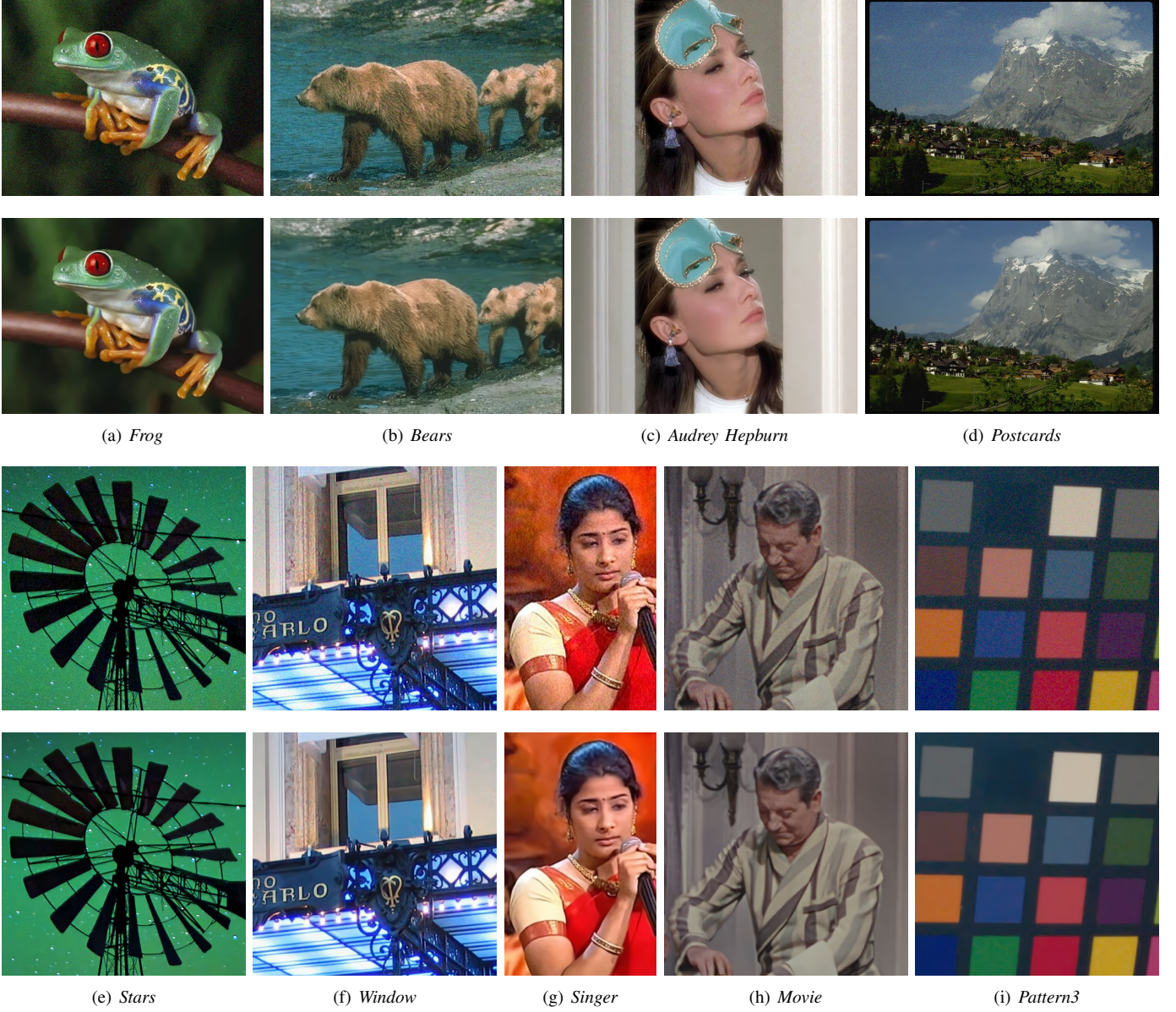


Fig. 11. More denoising results of FFDNet on real image denoising. (a)  $\sigma = 15$ ; (b)  $\sigma = 15$ ; (c)  $\sigma = 10$ ; (d)  $\sigma = 15$ ; (e)  $\sigma = 18$ ; (f)  $\sigma = 15$ ; (g)  $\sigma = 30$ ; (h)  $\sigma = 12$ ; (i)  $\sigma = 25$ .

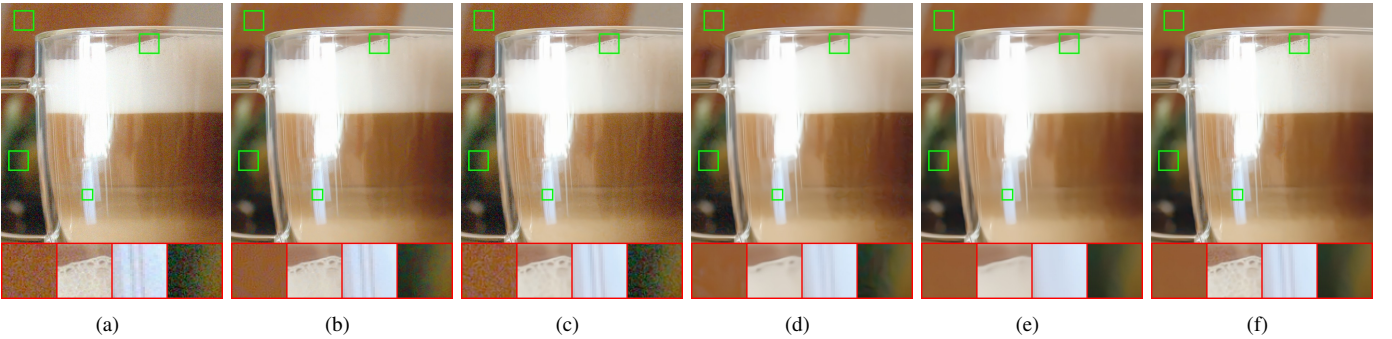


Fig. 12. An example of FFDNet on image “Glass” with spatially variant noise. (a) Noisy image; (b) Denoised image by Noise Clinic; (c) Denoised image by FFDNet with  $\sigma = 10$ ; (d) Denoised image by FFDNet with  $\sigma = 25$ ; (e) Denoised image by FFDNet with  $\sigma = 35$ ; (f) Denoised image by FFDNet with non-uniform noise level map.

- 2003.
- [11] K. Dabov, A. Foi, V. Katkovnik, and K. Egiazarian, "Image denoising by sparse 3-D transform-domain collaborative filtering," *IEEE Transactions on Image Processing*, vol. 16, no. 8, pp. 2080–2095, 2007.
  - [12] J. Mairal, F. Bach, J. Ponce, G. Sapiro, and A. Zisserman, "Non-local sparse models for image restoration," in *IEEE International Conference on Computer Vision*, 2009, pp. 2272–2279.
  - [13] W. Dong, L. Zhang, G. Shi, and X. Li, "Nonlocally centralized sparse representation for image restoration," *IEEE Transactions on Image Processing*, vol. 22, no. 4, pp. 1620–1630, 2013.
  - [14] M. Elad and M. Aharon, "Image denoising via sparse and redundant representations over learned dictionaries," *IEEE Transactions on Image Processing*, vol. 15, no. 12, pp. 3736–3745, 2006.
  - [15] J. Mairal, M. Elad, and G. Sapiro, "Sparse representation for color image restoration," *IEEE Transactions on Image Processing*, vol. 17, no. 1, pp. 53–69, 2008.
  - [16] A. Buades, B. Coll, and J.-M. Morel, "A non-local algorithm for image denoising," in *IEEE Conference on Computer Vision and Pattern Recognition*, vol. 2, 2005, pp. 60–65.
  - [17] Y. Chen and T. Pock, "Trainable nonlinear reaction diffusion: A flexible framework for fast and effective image restoration," *IEEE Transactions on Pattern Analysis and Machine Intelligence*, vol. 39, no. 6, pp. 1256–1272, 2017.
  - [18] H. C. Burger, C. J. Schuler, and S. Harmeling, "Image denoising: Can plain neural networks compete with BM3D?" in *IEEE Conference on Computer Vision and Pattern Recognition*, 2012, pp. 2392–2399.
  - [19] V. Jain and S. Seung, "Natural image denoising with convolutional networks," in *Advances in Neural Information Processing Systems*, 2009, pp. 769–776.
  - [20] K. Zhang, W. Zuo, Y. Chen, D. Meng, and L. Zhang, "Beyond a Gaussian denoiser: Residual learning of deep CNN for image denoising," *IEEE Transactions on Image Processing*, vol. 26, no. 7, pp. 3142–3155, July 2017.
  - [21] A. Barbu, "Training an active random field for real-time image denoising," *IEEE Transactions on Image Processing*, vol. 18, no. 11, pp. 2451–2462, 2009.
  - [22] K. G. Samuel and M. F. Tappen, "Learning optimized MAP estimates in continuously-valued MRF models," in *IEEE Conference on Computer Vision and Pattern Recognition*, 2009, pp. 477–484.
  - [23] J. Sun and M. F. Tappen, "Learning non-local range markov random field for image restoration," in *IEEE Conference on Computer Vision and Pattern Recognition*, 2011, pp. 2745–2752.
  - [24] U. Schmidt and S. Roth, "Shrinkage fields for effective image restoration," in *IEEE Conference on Computer Vision and Pattern Recognition*, 2014, pp. 2774–2781.
  - [25] S. Lefkimmiatis, "Non-local color image denoising with convolutional neural networks," in *IEEE Conference on Computer Vision and Pattern Recognition*, 2017, pp. 3587–3596.
  - [26] J. Xie, L. Xu, and E. Chen, "Image denoising and inpainting with deep neural networks," in *Advances in Neural Information Processing Systems*, 2012, pp. 341–349.
  - [27] F. Agostinelli, M. R. Anderson, and H. Lee, "Robust image denoising with multi-column deep neural networks," in *Advances in Neural Information Processing Systems*, 2013, pp. 1493–1501.
  - [28] S. Ioffe and C. Szegedy, "Batch normalization: Accelerating deep network training by reducing internal covariate shift," in *International Conference on Machine Learning*, 2015, pp. 448–456.
  - [29] F. Yu and V. Koltun, "Multi-scale context aggregation by dilated convolutions," in *International Conference on Learning Representations*, 2016.
  - [30] V. Santhanam, V. I. Morariu, and L. S. Davis, "Generalized deep image to image regression," in *IEEE Conference on Computer Vision and Pattern Recognition*, 2017, pp. 5609–5619.
  - [31] A. Krizhevsky, I. Sutskever, and G. E. Hinton, "ImageNet classification with deep convolutional neural networks," in *Advances in neural information processing systems*, 2012, pp. 1097–1105.
  - [32] W. Shi, J. Caballero, F. Huszar, J. Totz, A. P. Aitken, R. Bishop, D. Rueckert, and Z. Wang, "Real-time single image and video super-resolution using an efficient sub-pixel convolutional neural network," in *IEEE Conference on Computer Vision and Pattern Recognition*, 2016, pp. 1874–1883.
  - [33] A. Levin and B. Nadler, "Natural image denoising: Optimality and inherent bounds," in *IEEE Conference on Computer Vision and Pattern Recognition*, 2011, pp. 2833–2840.
  - [34] D. Wang, P. Cui, M. Ou, and W. Zhu, "Deep multimodal hashing with orthogonal regularization," in *International Joint Conference on Artificial Intelligence*, 2015, pp. 2291–2297.
  - [35] Z. Mhammedi, A. Hellicar, A. Rahman, and J. Bailey, "Efficient orthogonal parametrisation of recurrent neural networks using householder reflections," *arXiv preprint arXiv:1612.00188*, 2016.
  - [36] K. Jia, "Improving training of deep neural networks via singular value bounding," in *IEEE Conference on Computer Vision and Pattern Recognition*, 2017, pp. 4344–4352.
  - [37] D. Xie, J. Xiong, and S. Pu, "All you need is beyond a good init: Exploring better solution for training extremely deep convolutional neural networks with orthonormality and modulation," in *IEEE Conference on Computer Vision and Pattern Recognition*, 2017, pp. 6176–6185.
  - [38] Y. Sun, L. Zheng, W. Deng, and S. Wang, "SVDNet for pedestrian retrieval," *arXiv preprint arXiv:1703.05693*, 2017.
  - [39] E. Vorontsov, C. Trabelsi, S. Kadoury, and C. Pal, "On orthogonality and learning recurrent networks with long term dependencies," *arXiv preprint arXiv:1702.00071*, 2017.
  - [40] J.-S. Lee, "Refined filtering of image noise using local statistics," *Computer graphics and image processing*, vol. 15, no. 4, pp. 380–389, 1981.
  - [41] J. Deng, W. Dong, R. Socher, L.-J. Li, K. Li, and L. Fei-Fei, "ImageNet: A large-scale hierarchical image database," in *IEEE Conference on Computer Vision and Pattern Recognition*, 2009, pp. 248–255.
  - [42] K. Ma, Z. Duanmu, Q. Wu, Z. Wang, H. Yong, H. Li, and L. Zhang, "Waterloo exploration database: New challenges for image quality assessment models," *IEEE Transactions on Image Processing*, vol. 26, no. 2, pp. 1004–1016, 2017.
  - [43] D. Kingma and J. Ba, "Adam: A method for stochastic optimization," in *International Conference for Learning Representations*, 2015.
  - [44] A. Vedaldi and K. Lenc, "MatConvNet: Convolutional neural networks for matlab," in *ACM Conference on Multimedia Conference*, 2015, pp. 689–692.
  - [45] M. Lebrun, M. Colom, and J.-M. Morel, "The noise clinic: A blind image denoising algorithm," *Image Processing On Line*, vol. 5, pp. 1–54, 2015. [Online]. Available: <http://demo.ipol.im/demo/125/>
  - [46] R. Franzen, "Kodak lossless true color image suite," source: <http://r0k.us/graphics/kodak>, vol. 4, 1999.
  - [47] L. Zhang, X. Wu, A. Buades, and X. Li, "Color demosaicking by local directional interpolation and nonlocal adaptive thresholding," *Journal of Electronic Imaging*, vol. 20, no. 2, pp. 1–15, 2011.
  - [48] [Online]. Available: <https://ni.neatvideo.com/home>
  - [49] C. Liu, R. Szeliski, S. B. Kang, C. L. Zitnick, and W. T. Freeman, "Automatic estimation and removal of noise from a single image," *IEEE Transactions on Pattern Analysis and Machine Intelligence*, vol. 30, no. 2, pp. 299–314, 2008.
  - [50] M. Colom, M. Lebrun, A. Buades, and J.-M. Morel, "A non-parametric approach for the estimation of intensity-frequency dependent noise," in *IEEE International Conference on Image Processing*, 2014, pp. 4261–4265.